Supporting Information

Alignment of Lone Pairs in a New Polar Material $Li_2Ti(IO_3)_6$ – Synthesis, Characterization and Functional Properties

Hong-Young Chang,[1] Sang Hwan Kim,[1] P. Shiv Halasyamani,[1,*] and Kang Min Ok[2,*]

[1]*Department of Chemistry, University of Houston, 136 Fleming Building, Houston, Texas 77204-5003, USA and*

[2]*Department of Chemistry, Chung-Ang University, 221 Heukseok-dong, Dongjak-gu, Seoul 155-756, Republic of Korea*

E-mail: psh@uh.edu, kmok@cau.ac.kr

CONTENTS

S1. Calculated and observed powder X-ray diffraction pattern for $Li_2Ti(IO_3)_6$.

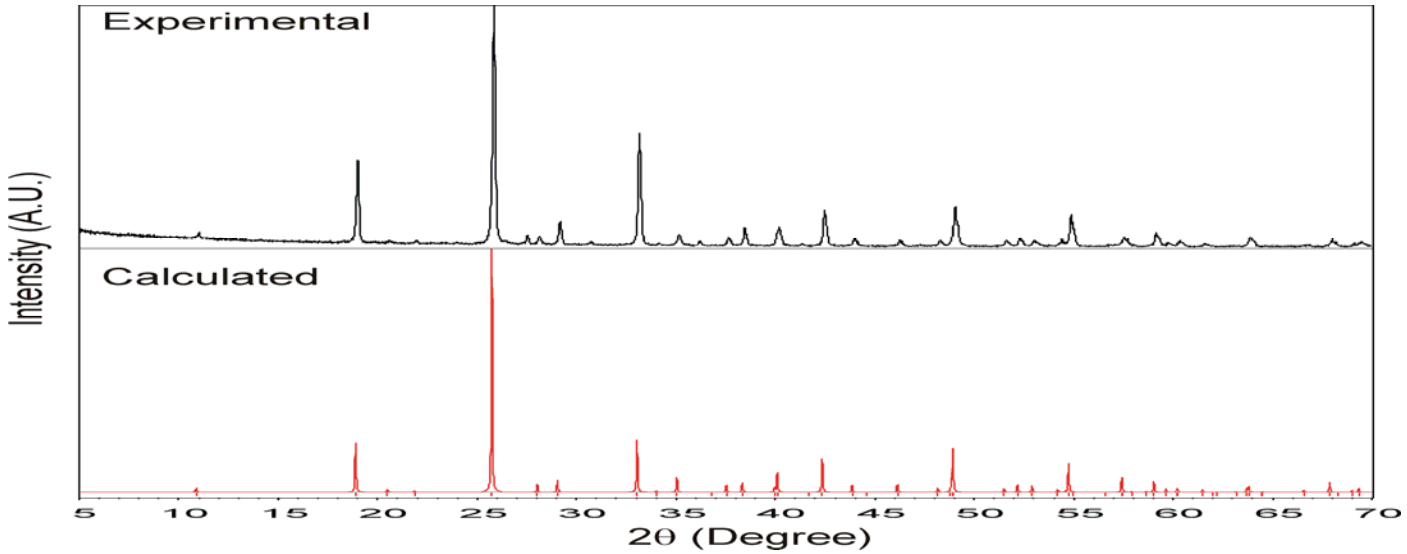

The X-ray powder diffraction data were collected on a PANalytical X'pert pro diffractometer using Cu Kα radiation in the 2θ range 5–70° with a step size of 0.008 degrees (°) and a scan time of 0.3 s/°. As shown in Figure S1, overall the observed patterns are well matched with the calculated pattern based on our single crystal data.

S2. TGA diagram for $Li_2Ti(IO_3)_6$.

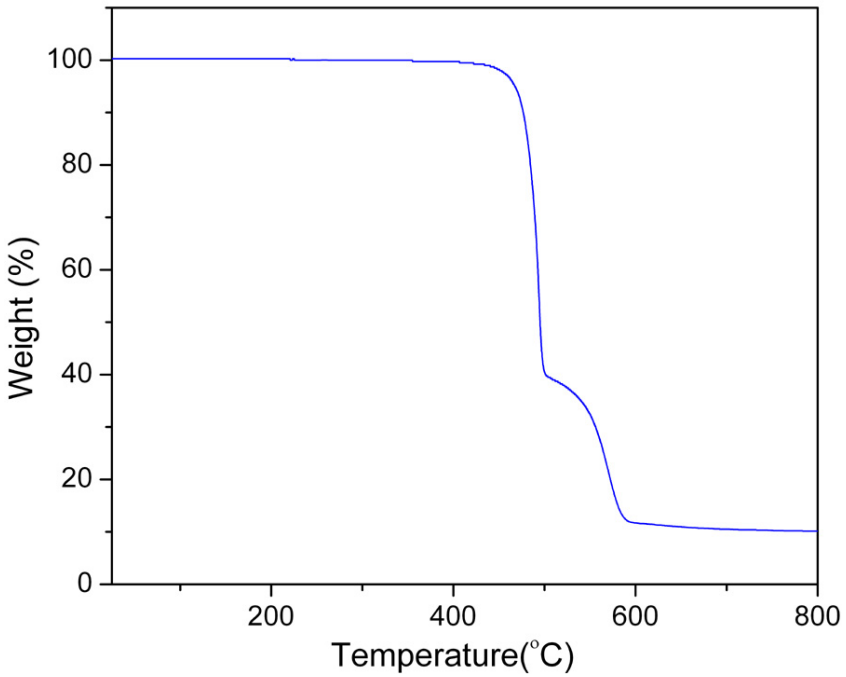

Thermogravimetric analyses (TGA) were carried out on a TGA 951 thermogravimetric analyzer (TA instruments). The sample was placed in a platinum crucible and heated at a rate of 10 °C min^{-1} from room temperature to 800 °C in a nitrogen flow. Figure S2 shows the TGA curve where the material is thermally decomposed through two steps exhibited at ~ 400 °C and ~ 490°C and finally, Li_2TiO_3 remains over 600 °C.

S3. Infrared spectrum for $Li_2Ti(IO_3)_6$.

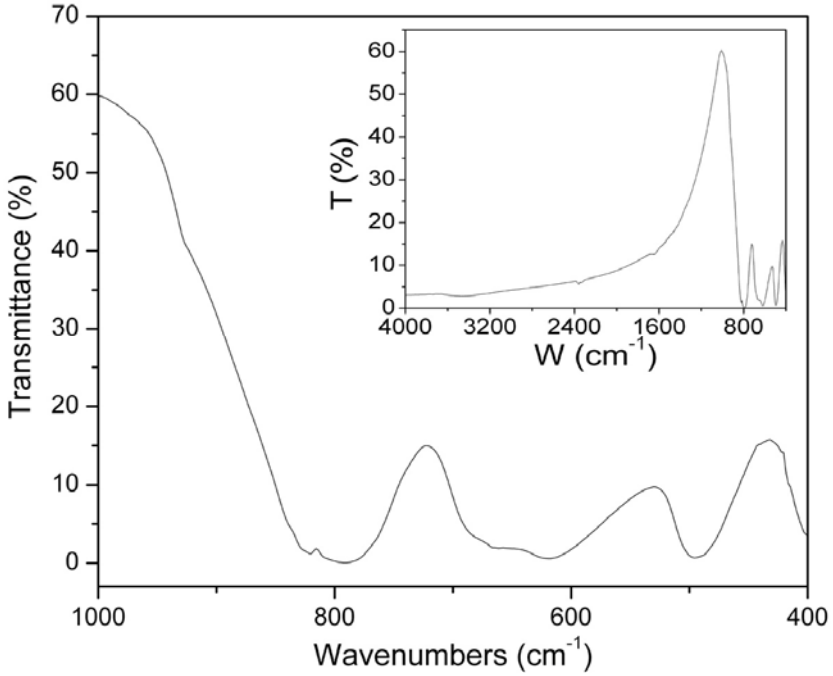

The Infrared spectrum was recorded on a Matteson FTIR 5000 spectrometer in the range of 400–4000cm^{-1}. The sample was pressed between two KBr pellets. The Infrared vibrations observed are assigned by ν(Ti-O): 729, 494 cm^{-1} and ν(I-O): 821, 661, 620 cm^{-1}. The assignments are consistent with those previously reported.[1] Inset shows the overall IR spectrum of $Li_2Ti(IO_3)_6$.

1. (a) Sykora, R. E.; Ok, K. M.; Halasyamani, P. S.; Albrecht-Schmitt, T. E. *J. Am. Chem. Soc.* **2002**, *124*, 1951. (b) Guarany, C. A.; Pelaio, L. H. Z.; Araujo, E. B.; Yukimitu, K.; Moraes, J. C. S.; Eiras, J. A. *J. Phys.: Condens. Matter* **2003**, *15*, 4851. (c) Ok, K. M.; Halasyamani, P. S *Inorg. Chem.* **2005**, *44*, 2263.

S4. Phase-matching, i.e., particle size vs SHG intensity, curve for $Li_2Ti(IO_3)_6$. The curve drawn is to guide the eye and is not a fit to the data.

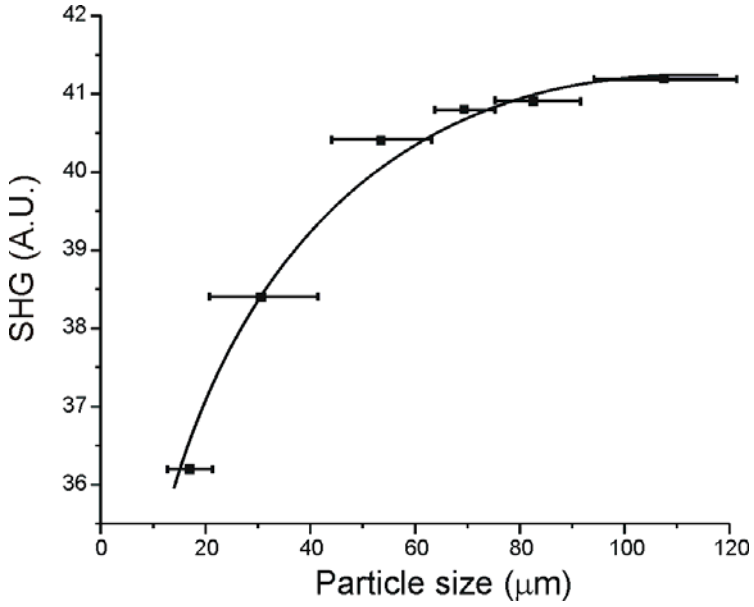

S5. Displacement vs. electric field loop for $Li_2Ti(IO_3)_6$.

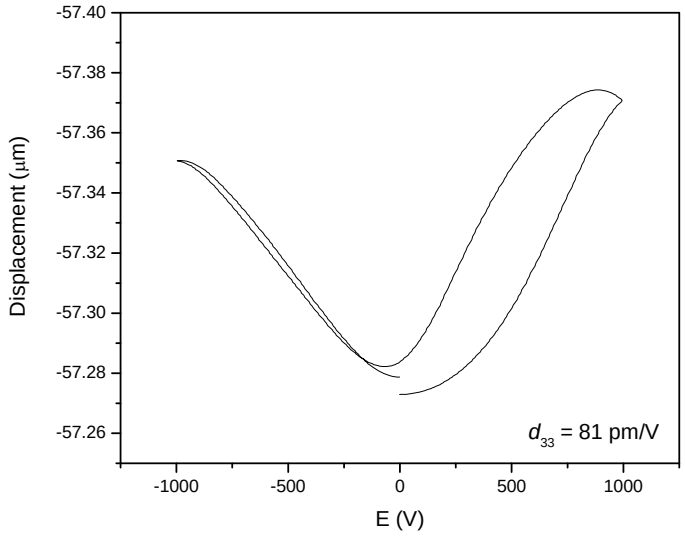

Converse piezoelectric measurements were performed using a Radiant Technologies RT66A piezoelectric test system with a TREK (model 609E-6) high-voltageamplifier, Precision Materials Analyzer, Precision High Voltage Interface, and MTI 2000 Fotonic Sensor. The material was pressed into 12-mm-diameter and ~ 0.5-mm-thick pellet sintered at 300 °C. Conducting silver paste was applied on both sides of the pellet surfaces for electrodes. A maximum voltage of 1000 V was applied to the sample.

Figure S4 shows the averaged displacement-vs.-electric field loop for $Li_2Ti(IO_3)_6$ after 20 measurements consecutively performed at the same condition. The piezoelectric charge constant, d_{33}, was calculated from

$$\Delta L = SL_0 - Ed_{33}L_0$$

where ΔL, L_0, S and E present the displacement of the sample, the sample thickness (m), the strain ($\Delta L/L_0$), and the electric field strength (V m^{-1}), respectively. The value of the piezoelectric charge constant d_{33} is estimated up to 81 pm/V.

S6. Polarization and pyroelectric data for $Li_2Ti(IO_3)_6$.

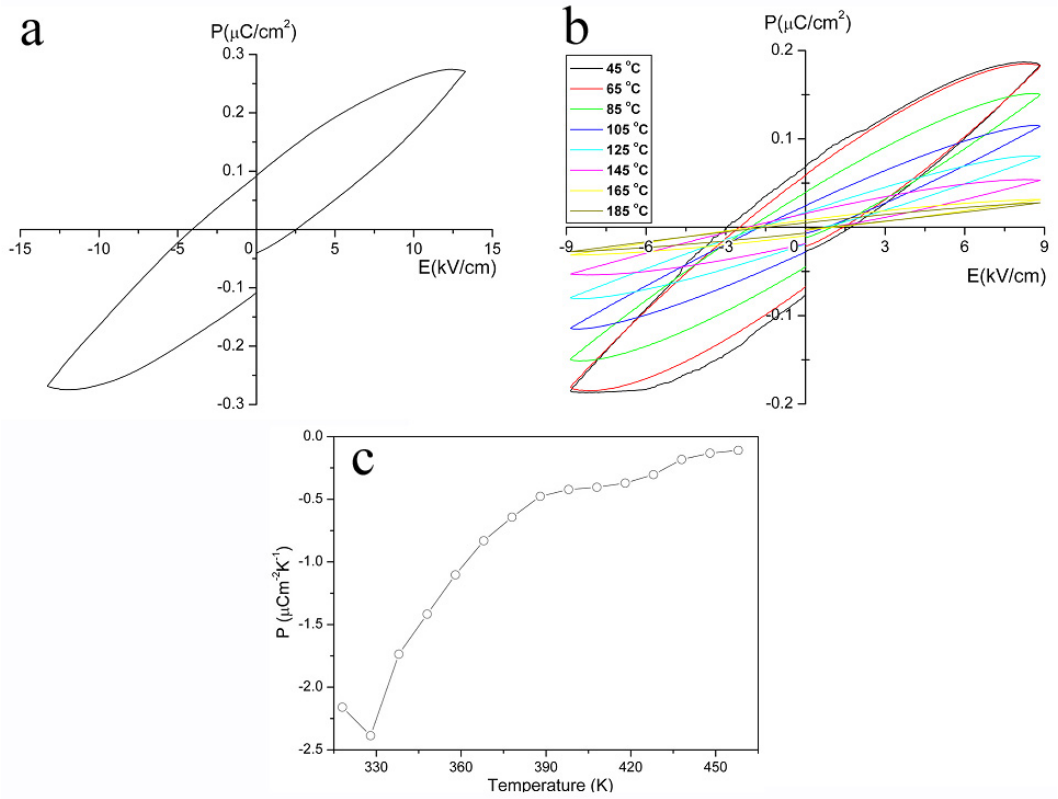

Ferroelectric hysteresis loops at different temperatures were measured on a Radiant Technologies RT66A ferroelectric test system with a TREK high voltage amplifier. The electrode-pasted sample as mentioned above was used for the measurements.

Although the polarization-vs.-electric field curve shown in Figure S5a reveals a 'hysteresis' loop, the observed loops are attributable to dielectric loss, i.e. 'leakiness', and not ferroelectric behavior. In Figure S5b, the temperature-dependent 'hysteresis' loops measured exhibit that the value of the remnant polarization decreases as temperature increases. A pyroelectric coefficient (p) of ~ -2.4 μC/m^{2}K at 55°C is shown in Figure S5c. This coefficient is on the order of tourmaline (-4.0 μC/m^{2}K).

S7. UV-vis diffuse reflectance spectrum for $Li_2Ti(IO_3)_6$

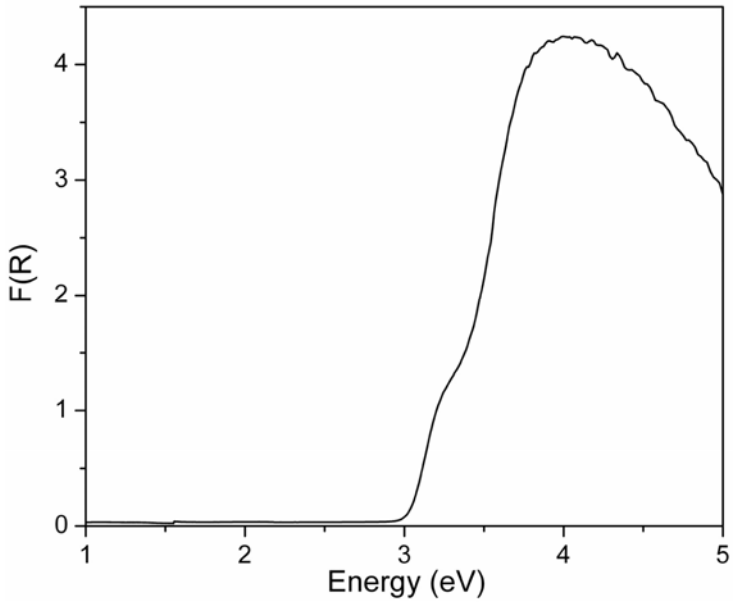

The UV-vis diffuse reflectance data were collected on a Varian Cary 500 scan UV-vis-NIR spectrophotometer over the spectral range 300-1500 nm at room temperature. Poly-(tetrafluoroethylene) was used as a reference material. Reflectance spectrum was converted to absorbance (K/S) with the Kubelka-Munk values $F(R)$ by following equation:

$$F(R) = \frac{(1-R)^2}{2R} = \frac{K}{S}$$

where R represents the reflectance, K the absorption, and S the scattering.

As seen in Figure S6, the onset of absorption at ~ 3.0 eV is obtained from extrapolating the linear part of the rising curve to zero. Additionally, another onset is observed ~ 3.3 eV.

S8. The TDOS and PDOSs plots from the Vanderbilt-type ultrasoft pseudo-potential calculations. The vertical line indicates the Fermi level, E_F. Black solid line: TDOS. Blue: Ti 3*d*. Green: I 5*s* PDOS. Red: I 5*p* PDOS. Orange: O 2*sp* PDOS.

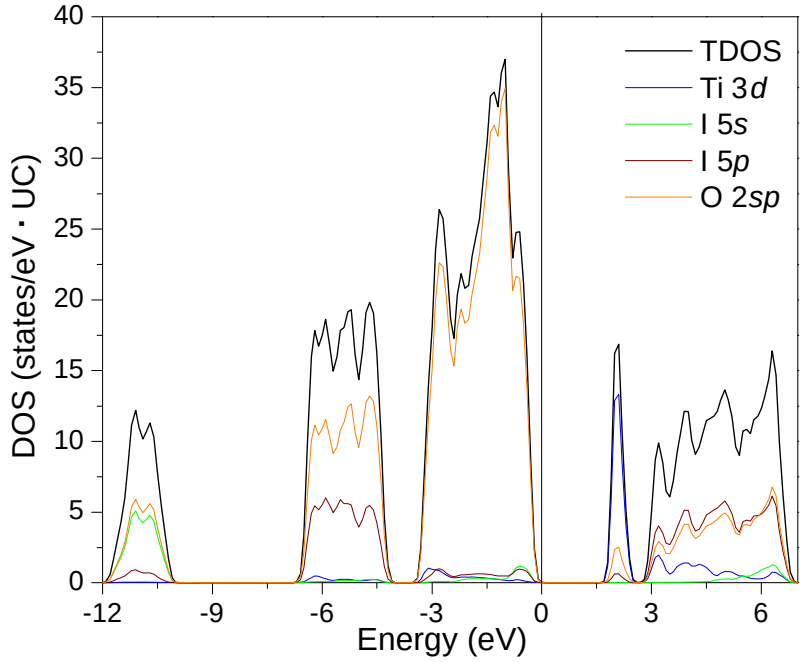

First principles density functional theory (DFT) electronic band structure calculations for the $Li_2Ti(IO_3)_6$ were performed by using the plane-wave pseudo-potential (PWPP) method as implemented in the Quantum-ESPRESSO package (version 4.0.1). The Perdew-Burke-Ernzerhof (PBE) exchange-correlation functional of a generalized gradient approximation (GGA) was employed with Vanderbilt-type ultrasoft (VU) and norm-conserving Martins–Troullier (MT) pseudo-potentials (PP) for the elements. The MT PPs generated from FHI-98 code are converted for the calculations. A plane wave energy cutoff was set to 37 Ry and a k-point grid of 5 × 5 × 9 was used for the Brilliouin zone integrations. A total energy convergence threshold was set to 10^{-6} Rydberg.

For the calculations, a disorder-free structure was adopted by lowering the symmetry to space group *P*3 (No. 143). The *P*3 model has the vacancy and the Ti atom alternating in an ordered manner along the *c*-direction. The volume of the structure is same with the volume determined expermimentally.

In Figure S7, the band structure from the VU-PP calculation shows an energy gap at the Fermi level (E_F) ~ 1.6 eV as indicative of a band gap material. There are three valence bands shown in lower, middle and high energy regions below the Fermi level (E_F). The projected density of states (PDOSs) analysis shows that the lower region has significant O-2*sp* and I-5*s* bands constribution with small amount I-5*p*. The middle is mainly

made up of O-2*p* and I-5*p*. In the high region, there are main contributions of O-2*p*. Despite of the small contribution of I-5*s* into the top of the high valence band, it originates from interctions between O-2*p* and I-5*s*, especially their antibonding interaction. Such a feature commonly exhibited has been argured when the lone pair of cation (Sn^{2+}, Pb^{2+}, Bi^{3+}) formed is primarily driven by the cation – anion (O^{2-}) covalent interaction mediated by the cation 5*p* due to SOJT effect.

The bands above E_F shows split narrow and broad conduction bands. The band splitting looks like t_{2g}-e_g splitting due to the Ti^{4+} sighlty distorted toward a face (C_3-type distortion) of its octahedron. The narrow band is mainly composed of Ti-(*dz*^{2}, *d*x^2-y^2, *d*xy) and while the broad consists of O-2*sp*, I-5*p*, and Ti-(*d*yz,*d*xz).

Although the energy band gap is underestimated approximately 1.4 eV, our band structure calcualtion results provide valuable semi-quantitative understanding of the optical spectrum. The two onsets of the absorption may be attributable to the two different conduction bands. For the 3.0 eV onset case, the optical band gap is caused by attributable to the ligand (O)-to-metal (Ti) charge transfer. While, another onset is attributable to mainly ligand (O)-to-ligand (O and I) charge transition.

The electron localization function (ELF) iso-surfaces is shown in Figure S9 where there is [001] projection view of the ELF visulatization for $Li_2Ti(IO_3)_6$ with $\eta = 0.9$ from the MT-PP calculations.

S9. [001] projection view of the electron localization function (ELF) for $Li_2Ti(IO_3)_6$ from the MT-PP calculations.

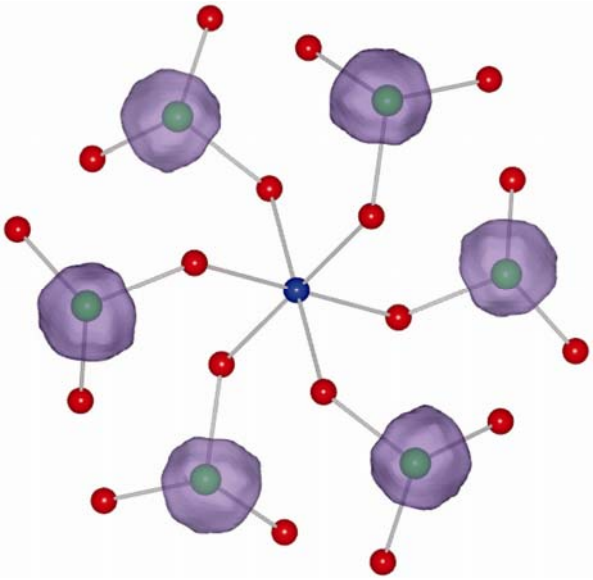

S10. Atomic coordinates and equivalent isotropic displacement parameters ($Å^2$) for $Li_2Ti(IO_3)_6$.

	x	y	z	U(eq)	Occ.
Li(1)	0.3333	0.6667	0.777(4)	0.017(8)	1.0
Ti(1)	0.0000	0.0000	0.8376(10)	0.014(1)	0.5
I(1)	0.6785(1)	0.6485(1)	0.7113(2)	0.017(1)	1.0
O(1)	0.8109(7)	0.8623(7)	0.5839(11)	0.027(2)	1.0
O(2)	0.5508(7)	0.7944(7)	0.0007(11)	0.020(1)	1.0
O(3)	0.4957(7)	0.6090(8)	0.5374(10)	0.020(1)	1.0

U(eq) is defined as one third of the trace of the orthogonalized U_{ij} tensor.

S11. Hypothetical polarization reversal for an IO_3 polyehdron.